Elaboration and properties of nanofibrillated cellulose composites with polypyrrole nanotubes or their carbonized analogs

Tomáš Lapka [1], Dušan Kopecký [1], Petr Mazúr [1], Jan Prokeš [2], Pavel Ulbrich [3], Marcela Dendisová [1], Michal Sedlačík [4], Fatima Hassouna [1]*

[(1)] Faculty of Chemical Engineering, University of Chemistry and Technology, Prague, 166 28 Prague 6, Czech Republic

[(2)] Faculty of Mathematics and Physics, Charles University, 180 00 Prague 8, Czech Republic

[(3)] Department of Biochemistry and Microbiology, University of Chemistry and Technology, Prague, 166 28 Prague 6, Czech Republic

[(4)] Centre of Polymer Systems, Tomas Bata University in Zlín, 760 01 Zlín, Czech Republic

Corresponding author:

Assoc. prof. Fatima Hassouna

Tel: +420220444099

E-mail: fatima.hassouna@vscht.cz

Abstract

Flexible electrically conductive composites based on renewable resources have recently attracted a growing interest for the development of high performance sustainable electronic and energy storage devices to meet the needs of modern wearable and portable electronics. In this study, electrically conductive flexible composite films based on nanofibrillated cellulose (NFC) and conductive nanotubular fillers were elaborated using environmentally friendly approach. Three conductive fillers were tested, specifically polypyrrole nanotubes (PPy-NT), carbonized polypyrrole nanotubes (C-PPy-NT) and commercially available multi-walled carbon nanotubes (MWCNT) for comparison. The prepared films were assessed for potential applications as electrodes for energy storage devices or protective shields for electromagnetic interference (EMI) shielding in the microwave region. Electrical conductivity measurement revealed that NFC films loaded with PPy-NT (PPy-NT/NFC) exhibited the highest conductivity (1.16 S cm^{-1}) compared to those loaded with C-PPy-NT or MWCNT. PPy-NT/NFC displayed the highest gravimetric capacitance among all tested films reaching 209.7 F g^{-1} at 10 mV s^{-1} in a stable potential window (from –0.5 to 0.15 V vs. MSE). When larger potential window (from –0.5 to 0.5 V vs. MSE) was applied, PPy-NT/NFC exhibited fast capacitance decay (to 80% of initial value in 50 cycles). Meanwhile, C-PPy-NT/NFC and MWCNT/NFC displayed significantly lower capacitances (below 20 F g^{-1} at 10 mV s^{-1}) but better cycling stability in a larger potential window. The highest shielding efficiency of all NFC-based composites was observed in case of PPy-NT/NFC, reaching 75 % in the C-band region.

Keywords:

Nanofibrillated cellulose; polypyrrole nanotubes; composites; electrochemical properties; energy storage; electromagnetic interference shielding

1. Introduction

Cellulose nanostructures, which are extracted from bacteria, higher plants, and algae have attracted a considerable attention in the frame of sustainable development as cellulose is the most abundant renewable resource on Earth. [1] Among them, nanofibrillated cellulose (NFC) displays excellent mechanical properties like high strength (up to 6 GPa) and high Young's modulus (up to 250 GPa) [2], outstanding optical properties and chemically reactive surface, which can be used to achieve tailorable functionalities. Thanks to these properties, mechanically strong, lightweight and flexible NFC-based composites in a form of aerogels or films can be synthesized when the nanofibers are interwoven. [1,3-8] Nanofibrillated cellulose acts as a renewable reinforcing agent or a mechanical skeleton capable of high deformation and, at the same time, as a useful template for tailoring functionalities. Due to the above mentioned facts and thanks to the increasing effort to develop environmentally friendly technologies, flexible conductive composites based on NFC have recently attracted a growing interest in the field of high performance sustainable wearable and portable electronic and energy storage devices. [9,10]

To date, three main material classes and their composites have been investigated for those applications: i) carbonaceous materials (*e.g.* graphene, carbon nanotubes, two-dimensional carbides and their derivatives); ii) metal oxides and iii) conducting polymers. [9,11,12]

Polypyrrole (PPy) is one of the most investigated conducting polymers. It exhibits high chemical stability, high values of DC electrical conductivity (typically units of S cm^{-1}) and complex permittivity (real part from tens to hundreds) [13,14], high specific mass capacitances and power densities [9,10,15,16] and aptitude to dissipate and attenuate electromagnetic waves in the frequency range from 300 kHz to 300 GHz (radio wave and microwave region) [13,14]. Furthermore, the low cost and easy synthesis of PPy in aqueous medium and simple functionalization with specific

groups combined with its excellent biocompatibility makes it suitable for various applications including energy conversion and storage, electromagnetic interference (EMI) shielding, sensor technology, catalysis, adsorbents for environmental protection, (nano)electronics and also tissue engineering and drug delivery in biology and medicine. [17,18]

Composite films or aerogels prepared by in situ polymerization of PPy on NFC have been recently used as electrodes in ion-exchange and paper-based energy storage devices. [9,16,19] They exhibited high gravimetric (127 F g^{-1}) and volumetric (122 F cm^{-3}) capacitances at high current densities (300 mA $cm^{-2} \approx 33$ A g^{-1}) with active mass loadings as high as 9 mg cm^{-2}. [19]

To the best of our knowledge, novel PPy nanostructures (nano- and micro- tubes, rods, wires, flakes, brushes, flowers, and similar, highly organized, uniform and reproducible structures) have not been incorporated into NFC to elaborate flexible conductive films yet, despite the fact that they excel over their non-structured counterparts in many physico-chemical properties.[20] In particular, PPy nanotubes (PPy-NT) which have tens to hundreds of nm in diameter and are several μm long, exhibit the higher electrical conductivity (~ tens to hundreds of S cm^{-1}), better long-term stability (months to years) and resistance against deprotonation compared to other structures.[20] Thanks to these intrinsic properties, PPy-NT exhibited high aptitude to reflect or absorb electromagnetic radiation in the C-band region covering the range from 5.85 to 8.2 GHz [21] and specific capacitance of 120 F g^{-1} at low potential sweep rate (5 mV s^{-1})[17].

In addition, carbonized polypyrrole nanotubes (C-PPy-NT) were identified as promising materials in the field of electrochemical capacitors[17], electrocatalysts[17] and gas sensors[22] thanks to their high surface nitrogen content, good balance between micro- and mesoporosity and relatively good conductivity[17,22].

Following these findings, the presented work focuses on preparation of free-standing electrically conductive films based on composite of NFC and PPy-NT synthesized by using a structure-guiding agent methyl orange or C-PPy-NT obtained by carbonization of PPy-NT at high temperatures. For comparison, composite films constituted of NFC and commercially available multi-walled carbon nanotubes (MWCNT) were also elaborated. The relationships among the chemical structure, morphology and properties of the films were investigated. The potential applicability of all films as electrodes for energy storage devices and protective shields in EMI shielding was evaluated.

2. Materials and Methods

2.1 Materials

Pyrrole, iron(III) chloride hexahydrate, methyl orange (Sodium 4-{[4-(dimethylamino)phenyl]diazenyl}benzene-1-sulfonate) were purchased from Sigma-Aldrich, NFC gel 3.5 wt. % was kindly provided by Weidmann. MWCNT were kindly gifted by Cheap tubes. All chemicals were used as received without any further purification.

2.2 Experimental Methods

2.2.1 Materials Preparation

Synthesis of Polypyrrole Nanotubes

PPy-NT was synthesized by oxidation of pyrrole with iron(III) chloride hexahydrate in a presence of methyl orange.[23] 600 mL of 2.5 mM methyl orange was mixed together with 2.1 mL of pyrrole. The solution was cooled to 5 ℃ and subsequently an oxidant solution of 8.12 g of iron(III) chloride hexahydrate with 69 mL of distilled water was added dropwise. The reaction mixture was then

stirred during 24 hours to allow a total conversion of pyrrole into PPy-NT. The black PPy-NT precipitate was thereafter filtered and purified via Soxhlet extraction with acetone. After purification, PPy was dried in vacuum at 40 °C over several days and milled using nano-mill (Tube Mill control, IKA) for 2 min at 20 000 rpm.

Carbonization of Polypyrrole Nanotubes

Carbonization of PPy-NT onto C-PPy-NT was carried out in a tube furnace at 650 °C at a heating rate of 10 °C min^{-1} and under nitrogen flow of 25 L h^{-1}. After that, C-PPy-NT was cooled spontaneously in the nitrogen stream until the temperature decreased under 100 °C. As previously reported, the temperature of 650 °C is crucial to allow complete carbonization[22]. When the carbonization temperature is higher, the yield of C-PPy-NT is substantially reduced.

Preparation of Composite Films

Composite films composed of NFC and conductive fillers (i.e. PPy-NT, C-PPy-NT or MWCNT) were prepared by physical blending approach followed by solution casting of the slurry[24]. First, the conductive filler was incorporated in an aqueous suspension of 1 wt. % NFC at a mass ratio of filler:NFC equal to 1:1. The mixture was sonicated using ultrasound probe Sonopuls HD 4050 (power of 40 W and amplitude of 80 %) for 30 min. Afterwards, the suspension was poured into a mould with a defined shape and dried at room temperature. The subsequent films were marked as PPy-NT/NFC, C-PPy-NT/NFC and MWCNT/NFC.

2.2.2 Characterization

X-Ray Photoelectron Spectroscopy

X-ray photoelectron spectroscopy (XPS) measurements were carried out using Omicron Nanotechnology X-ray photoelectron spectroscope composed of monochromatic radiation Al lamp (1486.7 eV) in the constant analyzer energy mode. The treatment of spectra was performed with CasaXPS software.

Thermogravimetric Analyzer

Thermogravimetric analyses (TGA) were carried out using Stanton-Redcroft TG 750 in nitrogen atmosphere (20 ml min^{-1}) at a heating rate of 10 °C min^{-1} from room temperature to 800 °C.

Fourier-transform Infrared Spectroscopy

The chemical characterization of the components was carried out using Fourier-transform infrared (FTIR) spectroscopy in transmission mode. Thermo Scientific Nicolet FTIR spectrometer Nexus 670, working with OMNIC Software was used. FTIR spectra of the powder materials in the KBr pellets were obtained, 128 scans were collected for each spectrum with a resolution of 4 cm^{-1}.

Transmission Electron Microscopy

Morphology of the NFC was investigated using a transmission electron microscope (TEM model JEM-1010 JEOL, Ltd) equipped with a CCD camera MegaView III Olympus SIS (Germany). About 10 μL of the aqueous dispersions of the NFC were applied to a copper electron microscopic grid, covered by very thin layer of carbon, left to adhere for about 5 min. Subsequently, the grid was placed on a drop of 1% uranyl acetate in ethanol for about 2 – 5 min to contrast the sample. Microscopy measurements have proceeded at an acceleration voltage of 80 kV.

Scanning Electron Microscopy

The microstructure of the fillers and the films was characterized using a scanning electron microscope (SEM model Mira 3 LMH, Tescan). In order to investigate the morphology of the films on the cross section, they were immersed in liquid nitrogen and then cryo-fractured. All samples were sputter coated with 8 nm thick gold layer and analyzed under 3 kV of accelerating voltage.

X-Ray Diffraction

The physical structure of pure components was analyzed using a θ-θ powder diffractometer X'Pert^3 Powder from PANalytical (Almelo) in Bragg-Brentano para-focusing geometry using wavelength CuKα radiation (λ = 1.5418 Å, U = 40 kV, I = 30 mA). Powder samples of approximately 200 mg were placed on zero-background (0-BG) Si-plates and measured using an ultrafast detector 1D PIXcel angular range 5 – 50° (2θ) and a counting time of 175.185 to step -1. The diffractograms were analyzed using HighScorePlus 4.0 software.

Measurement of DC Electrical Conductivity

Room temperature DC electrical conductivity of films was determined by a four-point method in the van der Pauw contact arrangement using a Keithley 6221 DC and AC Current Source, a Keithley 2001 Multimeter as a voltmeter and a Keithley 7001 Switch System equipped with a Keithley 7011-S Quad 1×10 Multiplexer.

Electrochemical Characterization

The electrochemical characterization of prepared composite films was performed in 3-electrode arrangement in 1 mol dm^{-3} H_2SO_4 electrolyte. The tested film was pressed onto a working glassy carbon disc electrode (12.6 mm^2 active area). Prior to the coating, the glassy carbon electrode was

thoroughly polished by grit papers of various grit size to obtain well-defined smooth surface. The tested film was firstly immersed into used electrolyte for 15 minutes before it was mounted into the working electrode holder. A mercurous sulphate reference electrode (MSE) with saturated K_2SO_4 inner electrolyte (0.65 V vs. SHE) and platinum sheet counter electrode were used.

Electrochemical properties of the films were tested by standard electrochemical methods, including cyclic voltammetry (CV) and galvanostatic cycling. Initially, we performed 50 CV cycles in a potential range from –0.5 V to 0.5 V vs. MSE (or –0.5 to 0.15 V vs. MSE in case of PPy-based composite) with scan rate of 50 mV s^{-1} to stabilize the electrochemical response of the system and assess the stability. Subsequently, series of 5 CV cycles were recorded in the same potential ranges for various scan rates (5, 10, 20, 50, 100 and 200 mV s^{-1}). Finally, a series of galvanostatic charge-discharge cycles in the same potential ranges was performed under different constant currents (0.2, 0.5, 1, 2, 5 and 10 mA). The electrochemical measurements were performed using potentiostat/galvanostat FRA EC-LAB SP-300 (Biologic).

The specific capacitance was evaluated from CV experiment following formula:

$$C_{sp} = \frac{\int_{E_{min}}^{E_{max}} \frac{I}{v} dE}{(E_{max} - E_{min}) \cdot m}$$

where v is a potential scan rate, m is mass of electrochemically active components in the film and E_{max} and E_{min} are the chosen potential boundaries of the integral. For C-PPy-NT and MWCNT, specific capacitance was calculated as an average value from values of oxidation and reduction part of CV curve within boundaries from –0.3 V to 0.3 V vs. MSE. For PPy, the boundaries were from –0.1 V to 0.1 V vs. MSE.

The specific capacitance was also evaluated from galvanostatic charge-discharge cycling experiment using this equation:

$$C_{\mathrm{sp}} = \frac{Q_{\max}}{(E_{\max} - E_{\min}) \cdot m}$$

where $Q_{\max}$ is the maximal charge at the discharge part of the curve, $E_{\max}$ and $E_{\min}$ are the potential limits of the galvanostatic cycle, m is the mass of electrochemically active material in the film.

Measurement of Shielding Efficiency

The shielding efficiency of the studied NFC composites was measured using a PNA-L network analyser (Agilent N5230A) and a rectangular waveguide (WR 137) in the C-band frequency range from 5.85 GHz to 8.2 GHz. Rectangular composite samples (size 34.85 × 15.80 mm) were inserted into the waveguide, completely filling in its cross-section. Intensity, as well as the phase of incident (I_0) and transmitted (I_T) electromagnetic signal, was measured, from which scattering parameter (S_{21}) was obtained.

$$S_{21}(\mathrm{dB}) = 20 \log \frac{I_T}{I_0} \quad (1)$$

S_{21} equals to the portion of the signal transmitted through the measured sample.

3. Results and Discussion

Morphology and Structural Properties of Nanofibrillated Cellulose and Fillers

Figure 1 gathers representative morphologies of PPy-NT, C-PPy-NT, MWCNT and NFC. According to SEM images, PPy-NT exhibits a nanotubular morphology several micrometers long with a diameter around 60 – 80 nm (**Figure 1a**). The morphology as well as the average diameter of PPy-NT were not affected by the carbonization onto C-PPy-NT (**Figure 1b**). The nanotubular

morphology of PPy-NT and C-PPy-NT indicates that the methyl orange played a role of a structure-guiding agent successfully and that the carbonization of the latter did not compromise its morphology. Similarly, MWCNT display nanotubular morphology with an average diameter of 10 – 20 nm.

It is important to note that nitrogen physisorption revealed that non-carbonized PPy-NT have relatively low specific surface area (SSA) ($S_{BET} \approx 75$ m^2 g^{-1}). Upon carbonization, the SSA increased by about 3 times ($S_{BET} = 211$ m^2 g^{-1})[22]. MWCNT have SSA comparable to that of C-PPy-NT, i.e. 223 m^2 g^{-1}.

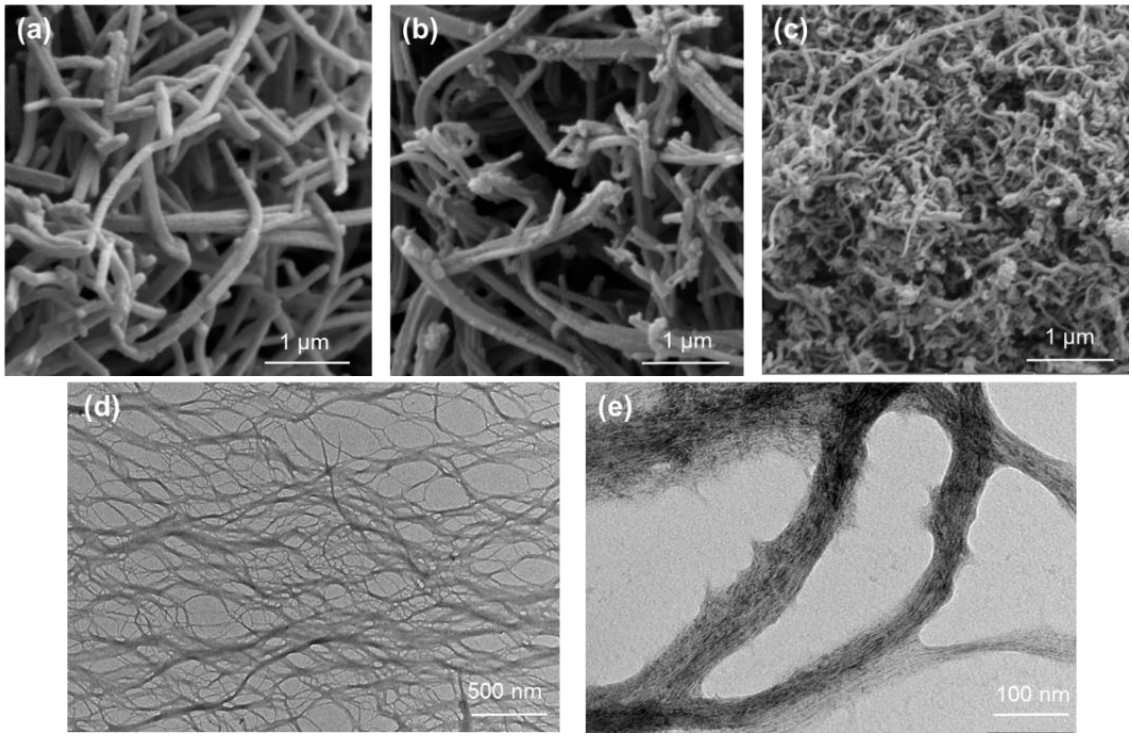

Figure 1: SEM images of a) PPy-NT, b) C-PPy-NT, c) MWCNT, d) and e) TEM images of NFC at various magnification

XRD analysis was carried out to complete the characterization of the physical structure of PPy-NT and C-PPy-NT. **Figure 2** shows XRD patterns of PPy-NT and C-PPy-NT powders. In the X-

ray pattern of PPy-NT, a large bump indicating that the polymer is in an amorphous state, and very weak diffraction peaks at 2θ = 18 and 25 °, attesting for the presence of residual crystals of methyl orange, can be observed. X-ray pattern of C-PPy-NT shows on the other hand a total absence of diffraction peaks due to the thermal decomposition of the residual crystalline methyl orange and the preservation of the amorphous nature of PPy-NT after carbonisation [25]. It is worth noting that as expected the X-ray pattern of MWCNT shows typical nanotubular graphitic peaks at 2θ = 26 and 44.5 ° assigned to the planes (002) and (101), respectively.[26]

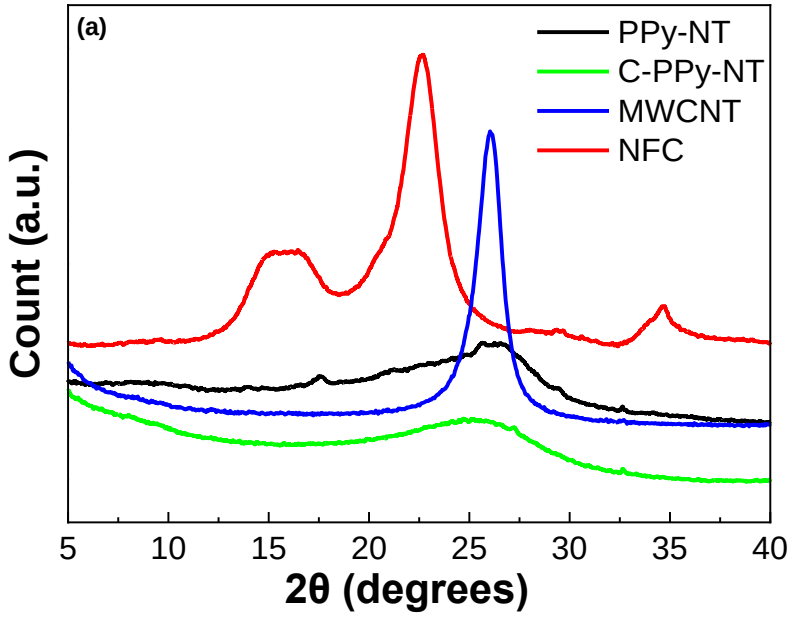

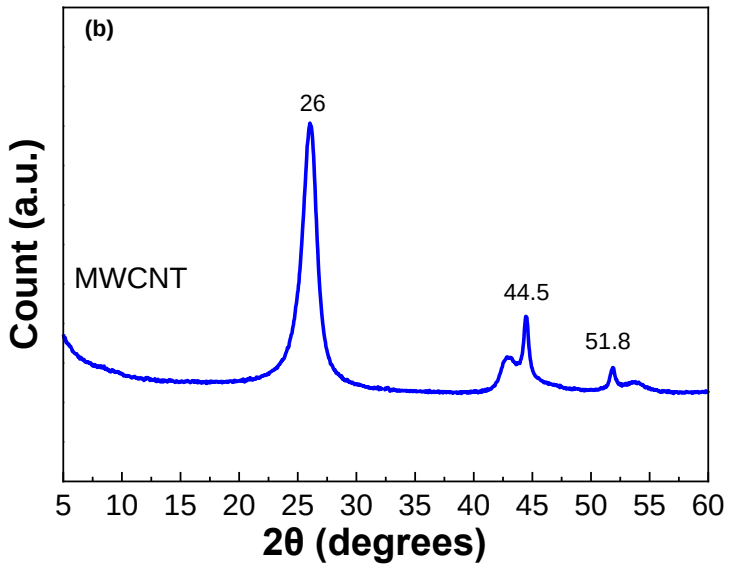

Figure 2: XRD patterns of a) PPy-NT, C-PPy-NT, MWCNT and NFC in the range of 2θ = 5 - 40, and b) MWCNT in the range of 2θ = 5 – 60 °

Differences in the chemical structure between PPy-NT and C-PPy-NT were also highlighted by FTIR analysis as a result of the carbonization process (**Figure 3a**). Characteristic absorption bands of PPy-NT at 1542, 1304, 1160, 1038 and 964 cm^{-1} are observed. The absorption band at 1542 cm^{-1} is assigned to C-C stretching vibrations of pyrrole ring. Those at 1304 cm^{-1} and 1160 cm^{-1} are attributed to C-H or C-N in-plane deformation modes, and 1038 and 964 cm^{-1} are assigned to C-H and N-H in-plane deformation vibrations and C-H out-of-plane deformation vibrations, respectively[20,22]. In the FTIR spectrum of C-PPy-NT, two large absorption bands with a maximum at 1598 and 1283 cm^{-1} can be observed. The first band is assigned to the C–C stretching vibrations in pyrrole ring and the second to C–N in-plane deformation modes. The spectrum shape is close to that of the carbon-like materials with the Raman-active D and G, which are generally inactive in FTIR spectra. However, in disordered materials, they become IR-active due to symmetry breaking the carbon network; nonetheless they are very weak and the spectra are

flat and nearly featureless[22]. The FTIR spectrum of the MWCNT (**Figure 3a** and **Figure S1**) is typical of that of carbon materials, where no presence of functional groups was detected.

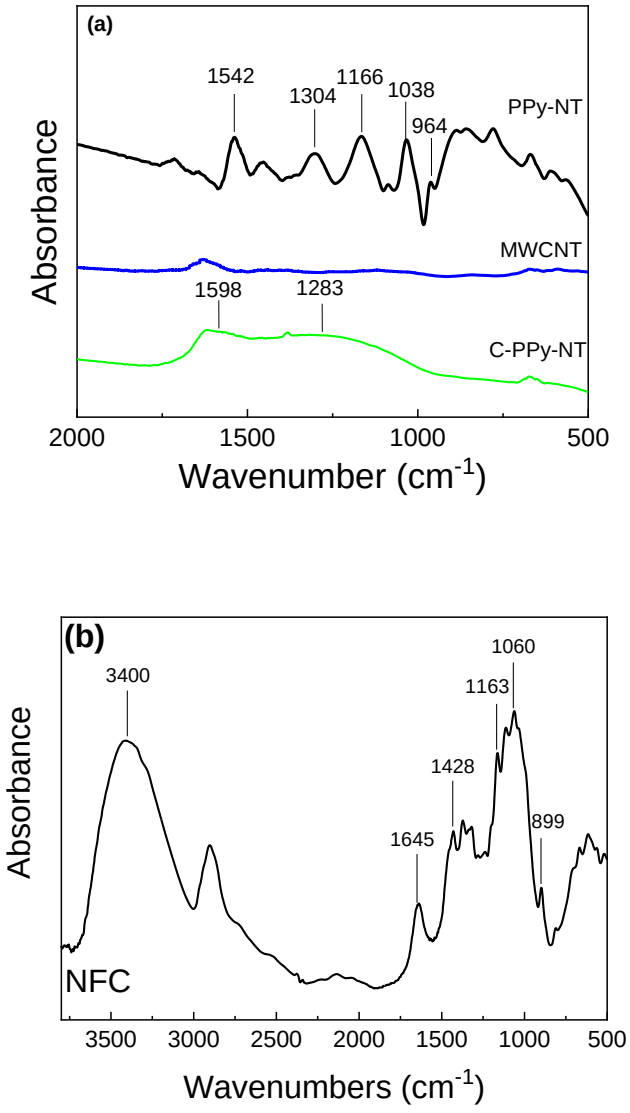

Figure 3: FTIR spectra of a) PPy-NT, C-PPy-NT and MWCNT in the region 800 – 2000 cm^{-1}, and b) NFC in the region 500 – 3800 cm^{-1}

Thermogravimetric analysis was carried out to better understand the carbonization process. PPy-NT displays three-stage degradation process, as shown in **Figure 4**, which corresponds well to the

thermal behavior of PPy-NT described in the literature. The first stage corresponding to a continuous release of moisture of about 5 % is in the temperature range 25 – 100 °C. The second stage of the degradation process involving the counter ions in the temperature range 150 – 400 °C. Finally, in the third stage, which occurs at a decomposition onset temperature of 620 °C, the polymer backbone is degraded. The total weight loss of PPy-NT up to 800 °C in nitrogen atmosphere reaches 55 wt. %[16,22,27] and about 60 wt. % at 650 °C, which corresponds to the carbonization temperature. In comparison with PPy-NT, C-PPy-NT exhibits much higher thermal stability due to its graphitic-like nature. Interestingly, the weight loss of about 3 % observed in C-PPY-NT in the temperature range 25 – 100 °C corresponding to moisture release confirms the hygroscopic nature of this filler. These findings are in agreement with FTIR results. Compared to C-PPy-NT, MWCNT exhibits hydrophobic nature characterized by the absence of moisture and similar thermal stability features.

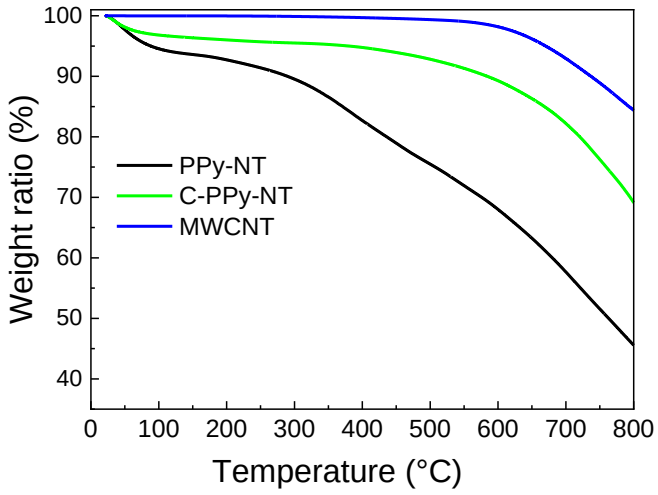

Figure 4: TGA curves of PPy-NT, C-PPy-NT and MWCNT under nitrogen atmosphere

The NFC employed in this work as a mechanical support that would be able to form a robust free-standing film was obtained by delamination of wood pulp by mechanical pressure processing[2,4].

The fibrillation allows anchoring a large amount of hydroxyl groups on the accessible pulp. TEM images in **Figure 1d** and **e** reveal that NFC exhibits a long fibrillary morphology with an average diameter of 35 nm. The length of the fibrils is very difficult to determine because of their high entanglement[28]. X-ray pattern (**Figure 2**) of NFC shows peaks at 2θ = 16.6, 22.6, and 34.7 degree attributed to (110), (200), and (004) planes, which is typical for cellulose-I structure[29]. FTIR analysis is in agreement with XRD as the FTIR spectrum of NFC (**Figure 3b**) shows absorption bands typical for cellulose bond stretching at 3400 cm^{-1} (-OH groups), 1645 cm^{-1} (C=O carbonyl groups), 1060 cm^{-1} (C-O-C glyosidic ether groups) and 1163 cm^{-1} (C-C ring breathing band).

Composite Materials

As mentioned above, composite films composed of NFC and conductive fillers (i.e. PPy-NT, C-PPy-NT, MWCNT) were prepared by physical blending approach followed by solution casting of the slurry at a ratio 1:1. In the **Figure 5,** photographs of NFC-based composite films are shown. The composites are in the form of black films with a thickness of approximately 140 μm. They are mechanically stable and they can be bent at an angle of ∼360° without breaking. However, it is important to note that the films with higher filler loadings exhibit lower flexibility. The morphology of the pristine NFC film and related composites was analyzed by means of SEM as shown in the **Figure 6**. Pristine NFC film displays a very compact structure characterized by interconnected nanofibers that results in a high mechanical performance. The SEM images provided the evidence that from microstructural point of view the dispersion of PPy-NT and C-PPy-NT in NFC leads to less compact and dense structure compared to pristine NFC, and also to the presence of an open, porous structure of entangled fibers. Both composites exhibited a

homogeneous dispersion of the filler in the NFC matrix thanks to the formation of intermolecular hydrogen bonds between amine groups of the filler and hydroxyl groups of NFC[30,31].

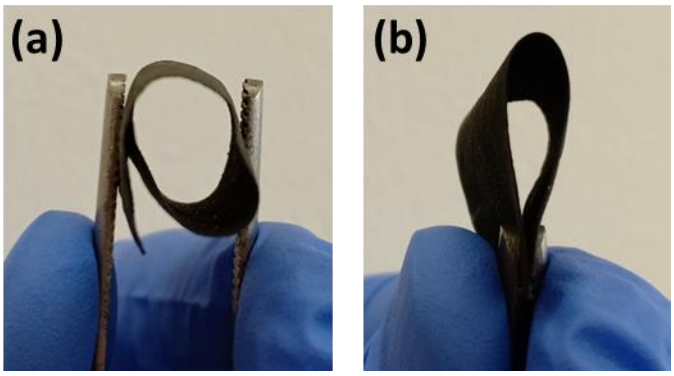

Figure 5. Representative photographs of the prepared NFC-based composite films

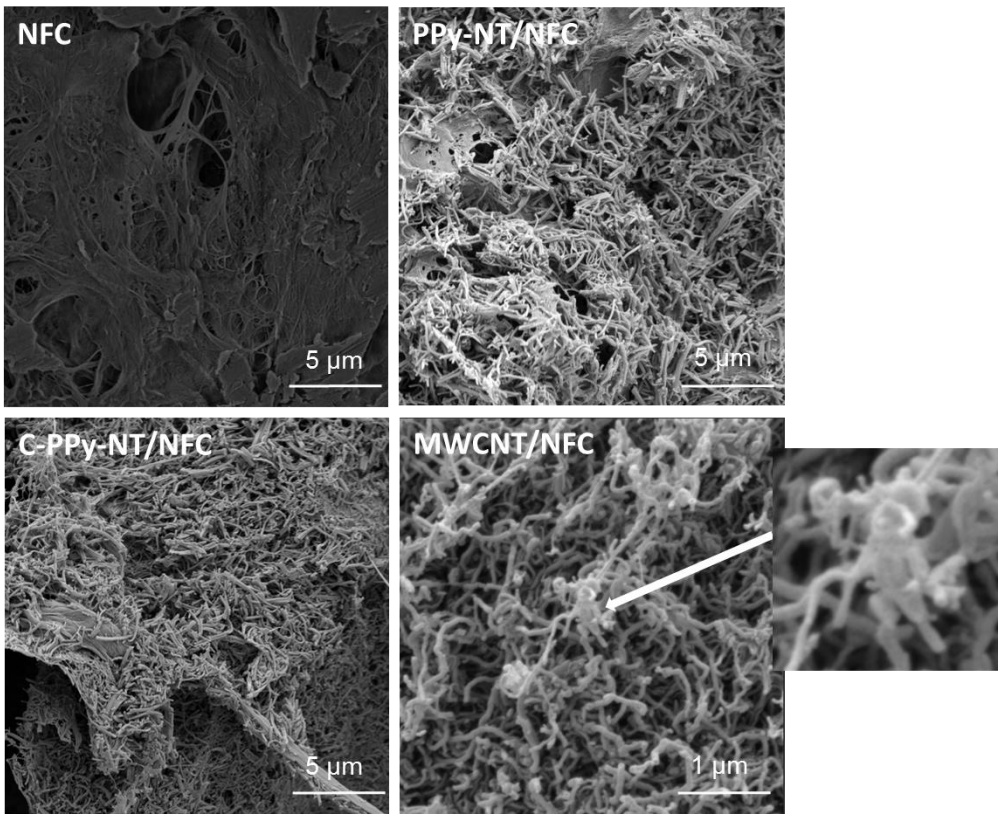

Figure 6: SEM images of pristine NFC, PPy-NT/NFC, C-PPy-NT/NFC and MWCNT/NFC

The electrical conductivities of PPy-NT, C-PPy-NT and their NFC-based composite films were measured to determine the possibility to apply them in electronics. For a sake of comparison, the electrical conductivity of a commercially available MWCNT and their related NFC-based film (i.e., MWCNT/NFC) was measured. The electrical conductivity values are summarized in **Table 1**. PPy-NT exhibit electrical conductivity of 50.9 S cm^{-1} which is slightly higher by a factor 1.3 than that of the commercial MWCNT (39.8 S cm^{-1}). On the other hand, upon carbonization, conductivity of C-PPy-NT is reduced by about 3 order of magnitude (8.2×10^{-2} S cm^{-1}).

The significant drop of the conductivity of PPy-CNT is caused by the loss of the polaron and bipolaron during the thermal decomposition of PPy-NT as highlighted by XPS analysis (**Figure S2, Table S1** and **Table 2**). **Figure S2** and **Table 2** summarize the proportion of the different chemical states of nitrogen functionalities evaluated by fitting the N(1s) core spectra. The deconvolution of N(1s) core level spectrum for PPy-NT shows the presence of three main peaks at binding energies of 399.47, 400.73 and 402.05 eV attributed to pyrollic nitrogen (-N-H-), protonated cation nitrogen (-N-$H^{+\cdot}$-), and protonated nitrogen (=N-H^{+}-), respectively [17,32]. The latter peak is not detected for PPy-NT, showing the absence of quaternary nitrogen which was reported previously in the literature[33]. In PPy-NT, binding energies of 398.19, 399.64, 400.68 and 401.64 eV attributed to pyridinic, pyrollic, graphitic and oxidized nitrogen, respectively, are detected.[34] Compared to PPy-NT, in C-PPy-NT the content of pyrrolic nitrogen is lower suggesting the transformation of pyrrolic form to pyridinic nitrogen. Comparable transformations of the carbon materials upon heating are also described in the literature. [33]

Table 1: Electrical conductivity of PPy-NT, C-PPy-NT, MWCNT and their NFC-based composite films

Sample	Electrical conductivity (S cm^{-1})
Fillers	
PPy-NT	50.9
C-PPy-NT	8.2×10^{-2}
MWCNT	39.8
Composites	
PPy-NT/NFC	1.16
C-PPy-NT/NFC	4×10^{-4}
MWCNT/NFC	0.44

Table 2: Summary of XPS data of PPy-NT and C-PPy-NT: proportion of N1s (%)[17,32,35]

Groups	Pyrollic N (-N-H-)	(-N-$\boldsymbol{H}^{+}$·-)	(=N-$\boldsymbol{H}^{+}$-)	Pyridinic N	Pyrollic N	Graphitic N	Oxidized N
Binding Energy (eV)	399.57	400.73	402.05	398.19	399.64	400.68	401.64
PPy-NT	67	23	10				-
C-PPy-NT				40	26	27	7

The conductivity values of the NFC-based composite films are lower compared to their conducting counterpart fillers due to the electrically insulating nature of NFC. As for PPy-NT, PPy-NT/NFC exhibits the higher electrical conductivity (1.16 S cm^{-1}) compared to C-PPy-NT/NFC (4×10^{-4} S cm^{-1}) and MWCNT/NFC (0.44 S cm^{-1}). Interestingly, though the conductivity of PPy-NT is only 1.3 times higher than that of MWCNT, the conductivity of related PPy-NT/NFC composite is 2.7 times higher than that of MWCNT/NFC. This observation can be explained by the formation of large aggregates of MWCNT (i.e., node-like structures) in MWCNT/NFC as can be seen in the SEM picture (**Figure 6)**. This is probably caused by the strong van der Waals interactions between the MWCNT and weaker interactions with NFC at the same time compared to PPy-NT.

Electrochemical Properties of the Composites

The electrochemical characterization of the NFC-based composite films, i.e., PPy-NT/NFC and C-PPy-NT/NFC was performed in a 3-electrode arrangement in 1 mol dm^{-3} H_2SO_4 electrolyte. Cyclic voltammetry and galvanostatic charge-discharge cycling was performed to assess the effect of the physico-chemical properties on their capacitive and redox characteristics. For a sake of comparison with carbonized nanotubes-based film (C-PPy-NT) obtained from the synthesized PPy-NT, we also characterized commercially available MWCNT/NFC films. Development of cyclovoltammograms within initial cycling of the individual films at 50 mV/s potential scan rate are presented in **Figure 7A**. Qualitatively, the CV curve of PPy-NT/NFC exhibits a characteristic redox behavior of PPy, with a broad oxidation peak at +0.19 V and a reduction peak at –0.10 V vs. MSE. Note that the NFC are electrochemically inactive (due to their insulating nature) and thus does not contribute to the measured electrochemical responses. However, this electrode, when cycled in broad potential range, exhibits a very fast changes of the CV features characterized by a significant decrease in the current intensity during the very first cycles indicating a lack of electrochemical stability of the PPy-NT in the composite film (**Figure 7A a).** This is in agreement with the literature reporting poor electrochemical instability of PPy-NT when cycled at potentials more positive than 0.6 V vs. Ag/AgCl reference electrode (i.e., 0.15 V vs. MSE).[36,37] In order to improve the stability the upper potential limit was decreased to 0.15 V vs. MSE and significant improvement of stability was achieved. In contrast, the PPy redox process is not observed in the CV of C-PPy-NT/NFC due to decomposition of PPy during the carbonization, which agrees well with the results of physicochemical characterization presented in previous sections (**Table 2**). The respective CV is close to an ideal capacitor *I*–*E* characteristics, being quasi-rectangular in shape and its current intensity even slightly increased during the cycling stability tests. This indicates the

slight increase of electrode-electrode interface area during the cycling, which might be due to a gradual electrolyte diffusion into the small pores of the nanostructured material.[38,39] Similar behavior was observed in the CV of MWCNT/NFC, indicating that C-PPy-NT behaves similarly to the commercial MWCNT. The summary of the evolution of the relative specific capacitances (i.e., a ratio between capacitance during the general cycle C_i over capacitance during the first cycle C_1) as a function of the number of cycles for all composite films is depicted in the **Figure 7B**. It shows a continuous capacitance decay along the cycling stability tests in the case of PPy-NT/NFC, when cycled in broader potential limits, while a slight increase of the capacitance is recorded in the case of C-PPy-NT/NFC and MWCNT/NFC. Thus the capacitance degradation of PPy-NT/NFC can be clearly attributed to the deterioration of redox process of PPy-NT and decrease of the upper potential limit to 0.15 V vs. MSE improves the cycling stability of the film, however for the price of reduced potential window of the application.

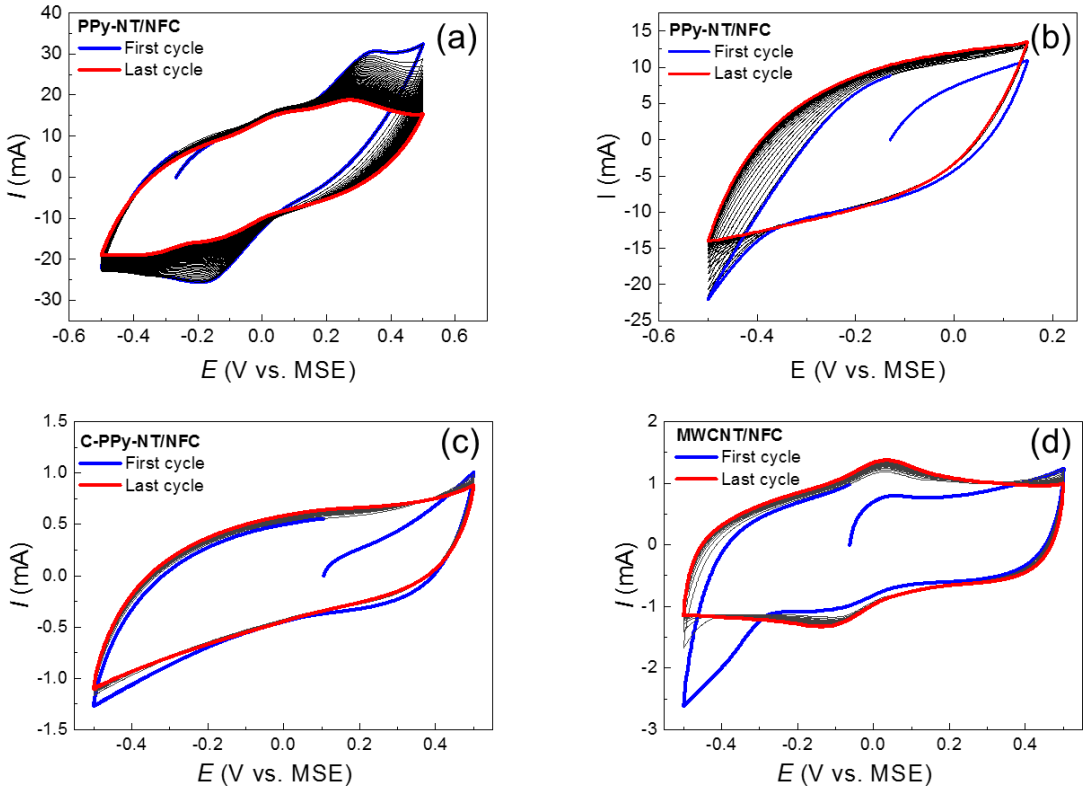

Figure 7A: Cyclic voltammograms of the composite films in 1M H_2SO_4 at 50 mV s^{-1} scan rate, 50 cycles.

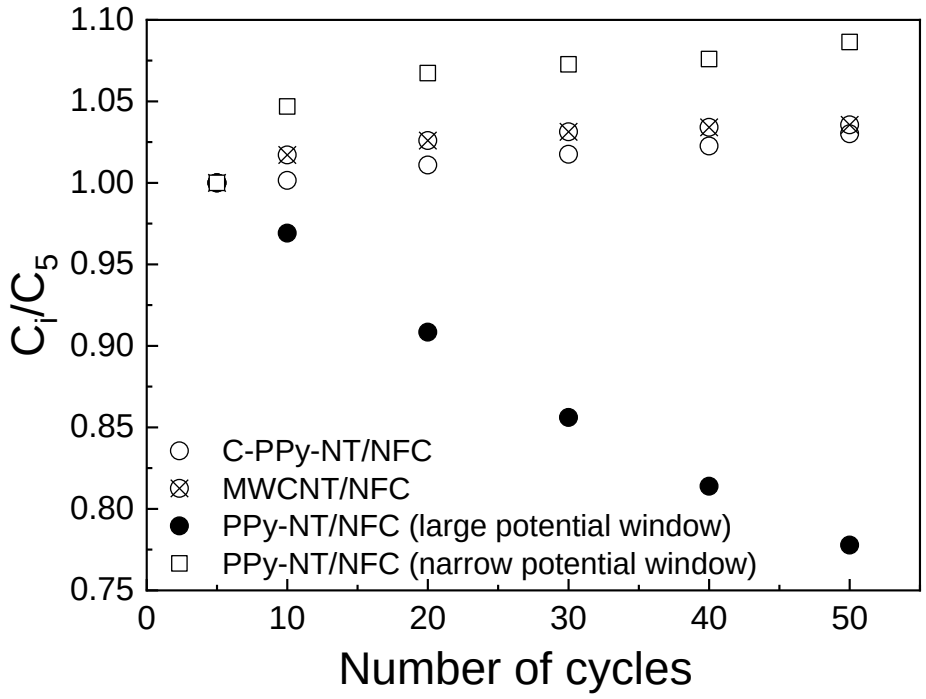

Figure 7B: Relative specific capacitance of the composite films as a function of the number of cycles evaluated form CV measurements at 50 mV s^{-1} in potential region –0.5 to 0.5 V vs. MSE (evaluated from Fig. 7A).

After the cycling stability tests, the composite films were characterized by CV under various scan rates, going from (200 to 5 mV s^{-1}) to assess the effect charging rate on the available capacitance of the films (**Figure S3 and Figure 8)**. The gravimetric capacitances are related to the mass of electrochemically active components of the film. As expected, all the composite films exhibit increasing values of specific capacitance for decreasing potential scan rates due to the reduced charge transfer and mass-transport polarization.[40-42]

PPy-NT/NFC displays the highest gravimetric capacitance among all composite films of 209.7 F g^{-1} at 10 mV s^{-1} and 59.9 F g^{-1} at 200 mV s^{-1} even when cycled in narrow potential window. In contrast, C-PPy-NT/NFC shows about one order lower gravimetric capacitances of about 18.2 F

g^{-1} at 10 mV s^{-1} and 4.6 F g^{-1} at 200 mV s^{-1}. Significantly lower gravimetric capacitances of C-PPy-NT/NFC can be explained by low electrical conductivity exhibited by the pristine C-PPy-NT, the absence of redox processes of PPy and relatively small electrode-electrolyte interface. On the other hand, the observed gravimetric capacitances are comparable to MWCNT/NFC (showing 17 F g^{-1} at 10 mV s^{-1} and 9.05 F g^{-1} at 200 mV s^{-1}) which exhibited much higher electric conductivity. The comparable performance of C-PPy-NT and commercial MWCNT in the NFC-based composites in terms of gravimetric capacitances could be explained by their comparable SSA (S_{BET} = 211 m^2 g^{-1} for C-PPy-NT and 223 m^2 g^{-1} for MWCNT) resulting in comparable area of electrode-electrolyte interface.[43] Besides the SSA, also the wettability of the sample by aqueous electrolyte related to the presence of polar functional groups on the surface of the carbonized fibers can significantly affect the real interfacial area. [44] It is envisioned in the future work to optimize the carbonization process of PPy and its activation in order to further optimize the SSA, wettability and electrical conductivity of the composite film. It is also envisioned to incorporate both PPy-NT and C-PPy-NT in one composite film to combine their advantages and enhance the overall electrochemical properties of the electrode.

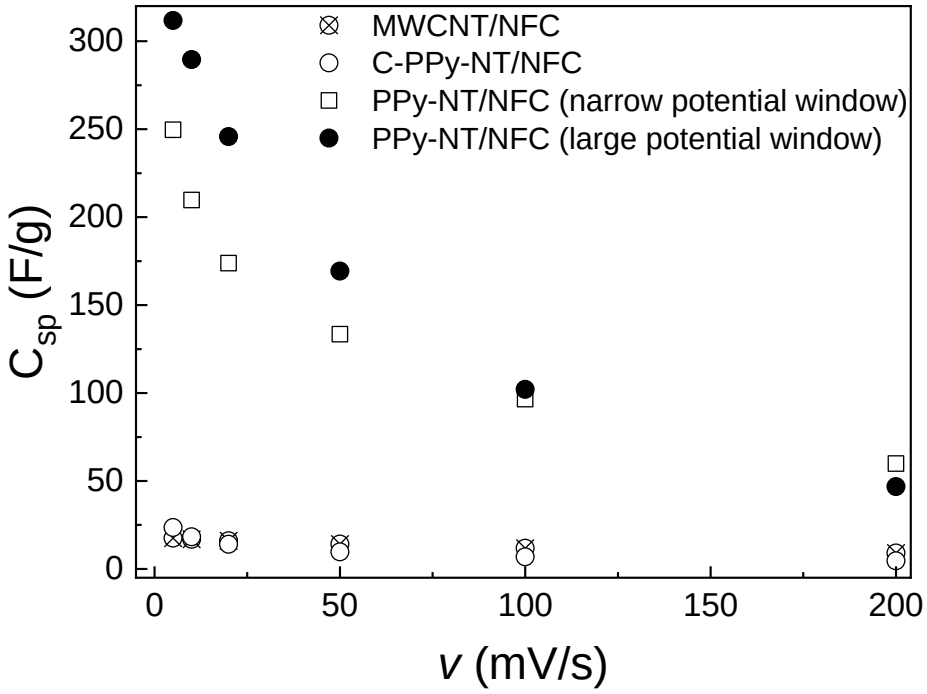

Figure 8: Specific capacitances of the films evaluated from cyclovoltammograms at different potential scan rates

The specific capacitance of the film was further studied by galvanostatic charge-discharge cycling curves at various currents ranging from 10 mA to 0.2 mA (**Figure S4** and **Figure 9)**. Analogically to the trend observed for CV measurements at various scan rates (**Figure 8**), specific capacitance decreases with increasing current due to charge transfer and mass transport limitation of the redox process of PPy. The non-monotonous trend of C_{sp}-I dependency for PPy-NT/NFC when cycled in broader potential window and its generally lower values (when compared to lower potential window) is most probably related to the fast degradation of PPy-NT/NFC upon the cycling. In accordance with the results from CV

measurements, the capacitance of C-PPy-NT/NFC and MWCNT/NFC is approx. of one order smaller.

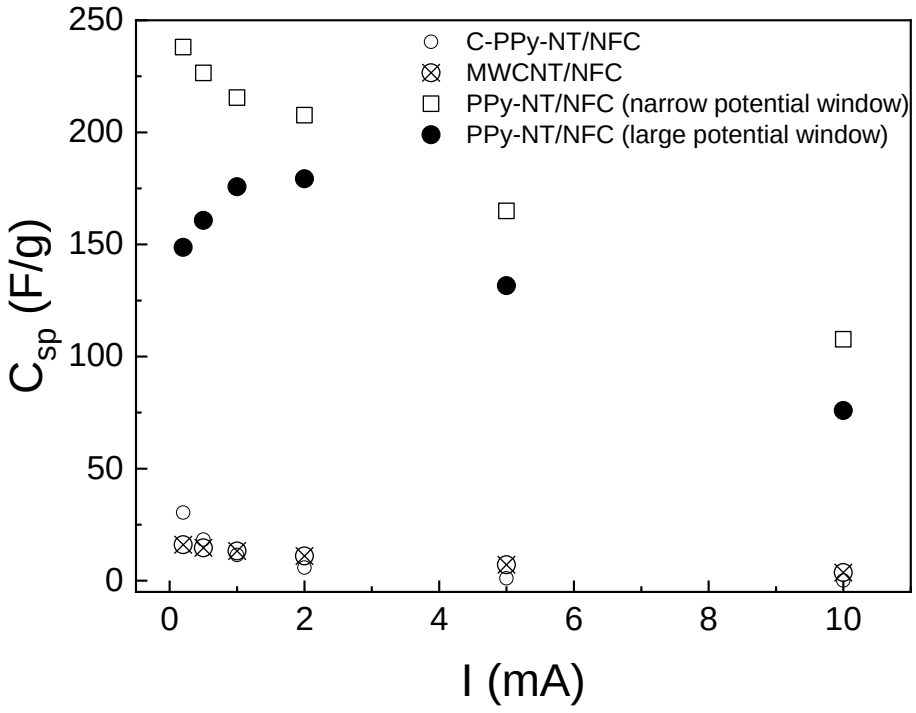

Figure 9: Specific capacitance of the films evaluated from galvanostatic charge-discharge cycling at various currents (0.2 – 10 mA range, the corresponding E-Q curves are presented in Figure S4).

Electromagnetic Interference Shielding Properties

Besides the electrochemical features, conducting polymers are well known materials in the field of EMI shielding due to their ability to absorb rather than reflect incoming electromagnetic radiation.[14] Moreover, they exhibit lower density, higher flexibility and better processability compared to the classic metallic shields.[45,46] Conducting polymer PPy is in EMI applications usually used in the non-structured, so-called globular form.[13] However, a recent advent of new

synthetic routes allows to prepare various PPy one-, two- or three- dimensional nanostructures (nano- and micro- tubes, fibres, plates, barrels, etc.) with better mechanical, electrical and structural properties.[47] A special position among these synthetic routes has so-called soft-template method using various dyes as structure-guiding agents.[48] The most developed PPy nanostructure prepared by this method so far is PPy-NT.[20]

One-dimensional PPy structures seems to be very promising in the EMI shielding due to their high aspect ratio which allows to reach percolation threshold at lower concentration of PPy filler in a matrix.[49] Several attempts have been done in order to test one-dimensional PPy for the EMI shielding application. Hu et al.[50] tested shielding efficiency of PPy rods synthesized in the presence of indigo carmine in the range of 8 – 18 GHz; Xie et al.[49] experimented with helical PPy nanostructures in the range of 2 – 18 GHz and early attempts have been done also in the testing of PPy-NT in the range of 5.85 – 8.2 GHz.[51] PPy-NT were recently studied in more details by Moučka et al.[21,52] in the C-band range of 5.85 – 8.2 GHz. The shielding efficiency of the composite of PPy-NT dispersed in silicone matrix (at 5 wt. %) has reached almost 80 %. The weaknesses of such composite lie however in degraded mechanical properties at higher concentration of PPy-NT (over 5 wt. %) and generally higher thickness of the tested layer (2mm thick plate).

The ability of PPy-NT, PPy-CNT and MW-CNT NFC films to absorb EMI in the C-band region from 5.85 to 8.2 GHz has been tested in the presented work (**Figure 10**). All NFC films were compared at the same ratio of the filler to NFC (1:1). The use of NFC as a matrix for PPy-NT, PPy-CNT and MW-CNT fillers allows to work with a higher concentration of the filler (approx. 50 wt. %) and one order of magnitude thinner layer (in this case, approx. 140 μm) while maintaining the flexibility of the shield. According to the results in the **Figure 10**, the shielding efficiency can be sorted in a direction PPy-NT > MWCNT >> C-PPy-NT. The highest shielding

efficiency measured on PPy-NT/NFC film reaches almost 80 %. A similar trend can be observed, when compared to the DC electrical conductivities of NFC-based films in the **Table 1**. Therefore, the differences in shielding efficiency can be ascribed mainly to the magnitude of DC electrical conductivity. The SSA does not seem to play a key role in the EMI shielding efficiency of the NFC-based films since the SSA of PPy-NT is approximately 3 times lower than that of C-PPy-NT and MWCNT. This can be explained by the high conducting filler loading (i.e., fixed ratio of the filler to NFC is 1:1) which probably reduces the effect of the SSA.

The results displayed in the **Figure 10** seems to be very promising because the preparation of PPy-NT is relatively easier compared to the device-demanding preparation of MWCNT.

Carbonization of PPy-NT onto C-PPy-NT was intended as a cheap source of N-doped carbon nanotubes suitable to replace commercially available carbon nanotubes. Unfortunately, C-PPy-CNT failed in EMI shielding, mostly because of their too low DC electrical conductivity.

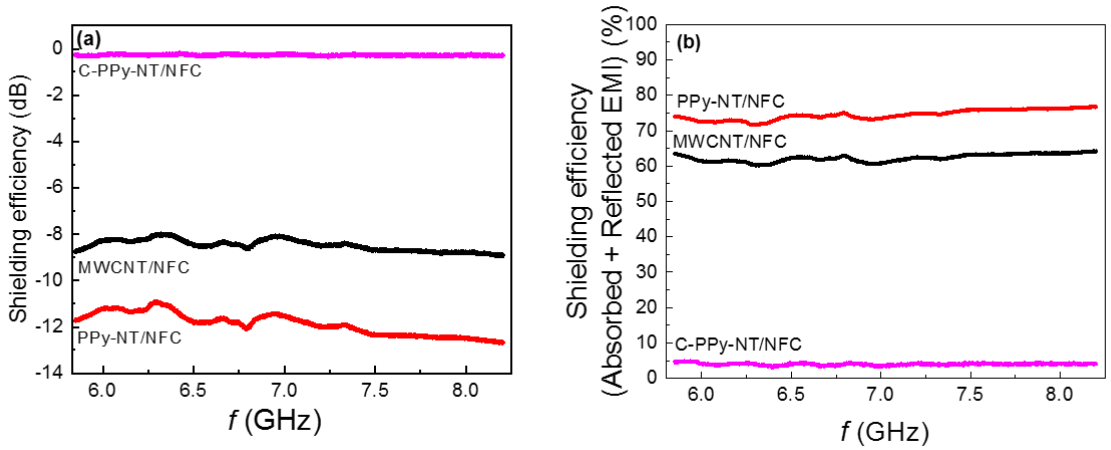

Figure 10: EMI shielding efficiency expressed by S_{21} parameter of PPy-NT/NFC, C-PPy-NT/NFC and MWCNT/NFC a) in dB and b) in %

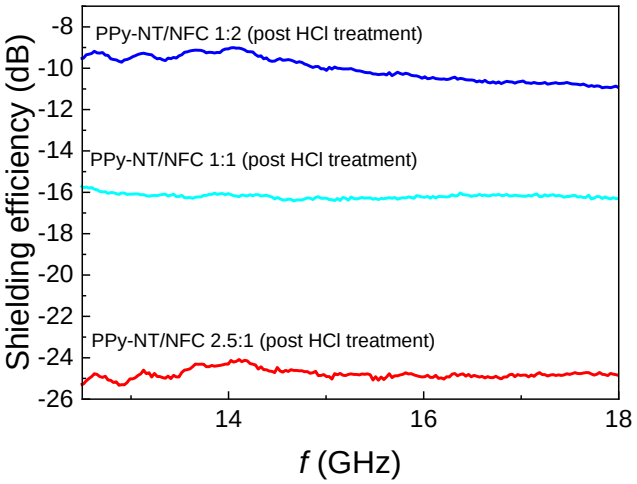

Table 3: Comparison of shielding effectiveness of various cellulose-based composites

Polymer composites	Thickness (µm)	Frequency (GHz)	EMI SE (dB) and in (%)*	Ref.
cellulose/CNT aerogel	2500	8.2–12.4	-20.8 (99.2)	[53]
PPy/NFC paper (in situ polymerisation, non-structured PPy)*	1000	8.2–12.4	−22 (99.4)	[54]
PANI/NFC paper	1000	8.2–12.4	−23 (99.5)	[55]
cellulose/CNT paper	450	15–40	−20 (-)	[56]
MWCNT/cellulose paper	170	0.5–1.0	−20.3 (99.1)	[57]
PPy /NFC paper	138	8–12	−23 (99.5)	[58]
Bacterial cellulose/PPy membrane		0.5–3.0	−15 (-)	[59]
Bacterial cellulose/PANI membrane	80	8.2–12.4	−5 (-)	[60]
PPy-NT/NFC (1:1) paper	140	5.85–8.2	−12 (74.9)	Current study
PPy-NT/NFC (1:1)-HCl post treatment paper	140	12.4-18	−16 (84.2)	Current study
PPy-NT/NFC (2.5:1) -HCl post treatment paper*	140	12.4-18	−25.3 (94.6)	Current study

* SE in parenthesis recalculated into % for the purpose of comparison

Conclusions

In this work, a simple, cost-effective and environmentally friendly strategy was used to elaborate electrically conductive composite films based on NFC employed as a renewable material and conductive nanotubular fillers. This strategy consists of physical blending in aqueous medium followed by the solution casting of the slurry. Three conductive fillers were tested, namely, PPy-NT synthesized by oxidation of pyrrole monomer with iron(III) chloride hexahydrate in the presence of azo dye methyl orange used as a structure-guiding agent, C-PPy-NT carbonized from PPy-NT at 650 °C in inert atmosphere and a commercially available MWCNT for comparison. The morphology, chemical structure and physico-chemical properties of the fillers and related composites were characterized and correlated. Both PPy-NT/NFC and C-PPy-NT/NFC exhibited a homogeneous dispersion of PPy-NT and C-PPy-NT in the NFC matrix, thanks to their chemical structure and morphology. The formation of intermolecular hydrogen bonds between amine groups of PPy-NT or C-PPy-NT and hydroxyl groups of NFC also played a role in the compatibilization of a filler with the NFC matrix. In contrast, large aggregates of MWCNT were observed in MWCNT/NFC caused probably by the strong van der Waals interactions between the MWCNT and weaker interactions with NFC. Electrical conductivity measurements showed that the conductivity values of the NFC-based composites are lower compared to their conducting counterpart fillers due to the electrically insulating nature of NFC. As for PPy-NT, PPy-NT/NFC displayed the highest electrical conductivity (1.16 S cm^{-1}) compared to C-PPy-NT/NFC (4×10^{-4} S cm^{-1}) and MWCNT/NFC (0.44 S cm^{-1}). Furthermore, PPy-NT/NFC film displayed the highest gravimetric capacitance among all the composite films between 209.7 F g^{-1} at 10 mV s^{-1} and 59.9 F g^{-1} at 200 mV s^{-1} and good cycling stability when upper potential was set to 0.15 V vs. MSE. After carbonization the capacitance of the PPy-based film dramatically decreased but it was still

comparable to the film based on commercially available MWCNT/NFC, both exhibiting better cycling stability at potentials above 0.15 V vs. MSE. Higher shielding efficiency of almost 80 % in the C-band region (5.85 – 8.2 GHz) was observed on PPy-NT/NFC compared to the NFC-based less conductive analogues, i.e. C-PPy-NT/NFC and MWCNT/NFC. Further, optimization of the material composition and the carbonization process of C-PPy-NT will be carried out to support further opportunities for the design in this emerging class of low-cost and environmentally friendly conductive composite films for application in flexible electronics and energy storage devices.

Conflicts of interest

There are no conflicts to declare.

Acknowledgements

The authors would like to thank Czech Science Foundation (GAČR No. 21-09830S) for the financial support. The authors would like to thank also the Specific university research (A2_FCHI_2021_003). We thank also European Regional development Fund-Project (ORGBAT) No.CZ.02.1.01/0.0/0.0/16_025/0007445 for the financial support of Dr. Mazúr.

References

1. Du X, Zhang Z, Liu W, Deng Y. Nanocellulose-based conductive materials and their emerging applications in energy devices - A review. Nano Energy. 2017;35:299-320.
2. Siqueira G, Bras J, Dufresne A. Cellulosic Bionanocomposites: A Review of Preparation, Properties and Applications. Polymers. 2010;2:728-765.
3. Moon RJ, Martini A, Nairn J, Simonsen J, Youngblood J. Cellulose nanomaterials review: structure, properties and nanocomposites. Chemical Society Reviews. 2011;40(7):3941-3994.

4. Kalia S, Dufresne A, Cherian BM, Kaith BS, Avéerous L, Njuguna J, Nassiopoulo E. Cellulose-Based Bio- and Nanocomposites: A Review. International Journal of Polymer Science. 2011;2011:1-35.
5. Tingaut P, Eyholzer C, Zimmermann T. Functional Polymer Nanocomposite Materials from Microfibrillated Cellulose. Advances in Nanocomposite Technology, Chapter 14, pages 319-334, Edited by Abbass Hashim, InTech, July, 2011, ISBN 978-953-307-347-7. (,).
6. Thomas B, Raj MC, B AK, H RM, Joy J, Moores A, Drisko GL, Sanchez C. Nanocellulose, a Versatile Green Platform: From Biosources to Materials and Their Applications. Chem Rev. 2018.
7. De France KJ, Hoare T, Cranston ED. Review of Hydrogels and Aerogels Containing Nanocellulose. Chemistry of Materials. 2017;29(11):4609-4631.
8. Kaushik M, Moores A. Review: nanocelluloses as versatile supports for metal nanoparticles and their applications in catalysis. Green Chemistry. 2016;18(3):622-637.
9. Nyholm L, Nystrom G, Mihranyan A, Stromme M. Toward flexible polymer and paper-based energy storage devices. Adv Mater. 2011;23(33):3751-3769.
10. Nishide H, Oyaizu K. Toward Flexible Batteries. Science. 2008;319(5864):737-738.
11. Simon P, Gogotsi Y, Dunn B. Where Do Batteries End and Supercapacitors Begin? Science. 2014;343(6176):1210-1211.
12. Peng X, Peng L, Wu C, Xie Y. Two dimensional nanomaterials for flexible supercapacitors. Chem Soc Rev. 2014;43(10):3303-3323.
13. Jiang D, Murugadoss V, Wang Y, Lin J, Ding T, Wang Z, Shao Q, Wang C, Liu H, Lu N, Wei R, Subramania A, Guo Z. Electromagnetic Interference Shielding Polymers and Nanocomposites - A Review. Polym Rev. 2019;59(2):280-337.
14. Kumar P, Narayan Maiti U, Sikdar A, Kumar Das T, Kumar A, Sudarsan V. Recent Advances in Polymer and Polymer Composites for Electromagnetic Interference Shielding: Review and Future Prospects. Polym Rev. 2019;59(4):687-738.
15. Novák P, Müller K, Santhanam KSV, Haas O. Electrochemically Active Polymers for Rechargeable Batteries. Chemical Reviews. 1997;97(1):207-282.
16. Nyström G, Mihranyan A, Razaq A, Lindström T, Nyholm L, Strømme M. A Nanocellulose Polypyrrole Composite Based on Microfibrillated Cellulose from Wood. The Journal of Physical Chemistry B. 2010;114(12):4178-4182.
17. Ćirić-Marjanović G, Mentus S, Pašti I, Gavrilov N, Krstić J, Travas-Sejdic J, Strover LT, Kopecká J, Moravková Z, Trchová M, Stejskal J. Synthesis, Characterization, and Electrochemistry of Nanotubular Polypyrrole and Polypyrrole-Derived Carbon Nanotubes. The Journal of Physical Chemistry C. 2014;118(27):14770-14784.
18. Vernitskaya TyV, Efimov ON. Polypyrrole: a conducting polymer; its synthesis, properties and applications. Russian Chemical Reviews. 1997;66(5):443-457.
19. Wang Z, Carlsson DO, Tammela P, Hua K, Zhang P, Nyholm L, Strømme M. Surface Modified Nanocellulose Fibers Yield Conducting Polymer-Based Flexible Supercapacitors with Enhanced Capacitances. ACS Nano. 2015;9(7):7563-7571.
20. Stejskal J, Trchová M. Conducting polypyrrole nanotubes: a review. Chem Pap. 2018;72(7):1563-1595.
21. Moučka R, Sedlačík M, Prokeš J, Kasparyan H, Valtera S, Kopecký D. Electromagnetic interference shielding of polypyrrole nanostructures. Synth Met. 2020;269:116573.
22. Kopecka J, Mrlik M, Olejnik R, Kopecky D, Vrnata M, Prokes J, Bober P, Moravkova Z, Trchova M, Stejskal J. Polypyrrole Nanotubes and Their Carbonized Analogs: Synthesis, Characterization, Gas Sensing Properties. Sensors. 2016;16(11).
23. Kopecká J, Kopecký D, Vrňata M, Fitl P, Stejskal J, Trchová M, Bober P, Morávková Z, Prokeš J, Sapurina I. Polypyrrole nanotubes: mechanism of formation. RSC Adv. 2014;4(4):1551-1558.

24. Hassouna F, Korbelářová J, Jaquet B, Kutorglo EM, Kopecký D, Ulbrich P, Fulem M, Hrdlička Z, Šoóš M. An environmentally benign methodology to elaborating polymer nanocomposites with tunable properties using core-shell nanoparticles and cellulose nanocrystals. Colloids and Surfaces A: Physicochemical and Engineering Aspects. 2018;553:169-179.
25. Chougule MA, Pawar SG, Godse PR, Mulik RN, Sen S, Patil VB. Synthesis and Characterization of Polypyrrole (PPy) Thin Films. Soft Nanoscience Letters. 2011;01(01):6-10.
26. Singh DK, Iyer PK, Giri PK. Diameter dependence of interwall separation and strain in multiwalled carbon nanotubes probed by X-ray diffraction and Raman scattering studies. Diamond Relat Mater. 2010;19(10):1281-1288.
27. Carrasco PM, Cortazar M, Ochoteco E, Calahorra E, Pomposo JA. Comparison of surface and bulk doping levels in chemical polypyrroles of low, medium and high conductivity. Surf Interface Anal. 2007;39(1):26-32.
28. Spence K, Habibi Y, Dufresne A (2011) Nanocellulose-Based Composites In: Kalia S, Kaith B, Kaur I (eds) Cellulose Fibers: Bio- and Nano-Polymer Composites Springer, Berlin, Heidelberg https://doiorg/101007/978-3-642-17370-7_7.
29. French AD. Idealized powder diffraction patterns for cellulose polymorphs. Cellulose. 2013;21(2):885-896.
30. Lay M, Méndez JA, Pèlach MÀ, Bun KN, Vilaseca F. Combined effect of carbon nanotubes and polypyrrole on the electrical properties of cellulose-nanopaper. Cellulose. 2016;23(6):3925-3937.
31. Müller D, Rambo CR, D.O.S.Recouvreux, Porto LM, Barra GMO. Chemical in situ polymerization of polypyrrole on bacterial cellulose nanofibers. Synth Met. 2011;161(1):106-111.
32. Han H, Cho S. Ex Situ Fabrication of Polypyrrole-Coated Core-Shell Nanoparticles for High-Performance Coin Cell Supercapacitor. Nanomaterials. 2018;8(9).
33. Morozan A, Jégou P, Campidelli S, Palacin S, Jousselme B. Relationship between polypyrrole morphology and electrochemical activity towards oxygen reduction reaction. Chemical Communications. 2012;48(38):4627-4629.
34. Tran T-N, Song MY, Singh KP, Yang D-S, Yu J-S. Iron–polypyrrole electrocatalyst with remarkable activity and stability for ORR in both alkaline and acidic conditions: a comprehensive assessment of catalyst preparation sequence. Journal of Materials Chemistry A. 2016;4(22):8645-8657.
35. Liang L, Chen G, Guo C-Y. 2017. Polypyrrole nanostructures and their thermoelectric performance. ed.
36. Mazeikiene R, Malinauskas A. Kinetics of the electrochemical degradation of polypyrrole. Polymer Degradation and Stability. 2002;75(2):255-258.
37. Otero TF, Ariza MJ. Revisiting the Electrochemical and Polymeric Behavior of a Polypyrrole Free-Standing Electrode in Aqueous Solution. The Journal of Physical Chemistry B. 2003;107(50):13954-13961.
38. Toh SY, Loh KS, Kamarudin SK, Daud WRW. Graphene production via electrochemical reduction of graphene oxide: Synthesis and characterisation. Chemical Engineering Journal. 2014;251(0):422-434.
39. Chakrabarti MH, Low CTJ, Brandon NP, Yufit V, Hashim MA, Irfan MF, Akhtar J, Ruiz-Trejo E, Hussain MA. Progress in the electrochemical modification of graphene-based materials and their applications. Electrochimica Acta. 2013;107(0):425-440.
40. Kroupa M, Offer GJ, Kosek J. Modelling of Supercapacitors: Factors Influencing Performance. Journal of The Electrochemical Society. 2016;163(10):A2475-A2487.
41. Yan H, Chunyi Z. Functional flexible and wearable supercapacitors. J Phys D: Appl Phys. 2017;50(27):273001.
42. Yan J, Wei T, Shao B, Fan Z, Qian W, Zhang M, Wei F. Preparation of a graphene nanosheet/polyaniline composite with high specific capacitance. Carbon. 2010;48(2):487-493.

43. Zheng W, Lv R, Na B, Liu H, Jin T, Yuan D. Nanocellulose-mediated hybrid polyaniline electrodes for high performance flexible supercapacitors. Journal of Materials Chemistry A. 2017;5(25):12969-12976.
44. Rabbow TJ, Whitehead AH. Deconvolution of electrochemical double layer capacitance between fractions of active and total surface area of graphite felts. Carbon. 2017;111:782-788.
45. Chung DDL. Materials for electromagnetic interference shielding. Mater Chem Phys. 2020;255:123587.
46. Wanasinghe D, Aslani F. A review on recent advancement of electromagnetic interference shielding novel metallic materials and processes. Composites Part B: Engineering. 2019;176:107207.
47. Valtera S, Prokeš J, Kopecká J, Vrňata M, Trchová M, Varga M, Stejskal J, Kopecký D. Dye-stimulated control of conducting polypyrrole morphology. RSC Adv. 2017;7(81):51495-51505.
48. Stejskal J, Prokeš J. Conductivity and morphology of polyaniline and polypyrrole prepared in the presence of organic dyes. Synth Met. 2020;264:116373.
49. Xie A, Wu F, Jiang W, Zhang K, Sun M, Wang M. Chiral induced synthesis of helical polypyrrole (PPy) nano-structures: a lightweight and high-performance material against electromagnetic pollution. Journal of Materials Chemistry C. 2017;5(8):2175-2181.
50. Hu S, Zhou Y, Zhang L, Liu S, Cui K, Lu Y, Li K, Li X. Effects of indigo carmine concentration on the morphology and microwave absorbing behavior of PPy prepared by template synthesis. Journal of Materials Science. 2018;53(4):3016-3026.
51. Babayan V, Kazantseva NE, Moučka R, Stejskal J. Electromagnetic shielding of polypyrrole–sawdust composites: polypyrrole globules and nanotubes. Cellulose. 2017;24(8):3445-3451.
52. Moučka R, Sedlačík M, Kasparyan H, Prokeš J, Trchová M, Hassouna F, Kopecký D. One-Dimensional Nanostructures of Polypyrrole for Shielding of Electromagnetic Interference in the Microwave Region. International journal of molecular sciences. 2020;21(22):8814.
53. Huang H-D, Liu C-Y, Zhou D, Jiang X, Zhong G-J, Yan D-X, Li Z-M. Cellulose composite aerogel for highly efficient electromagnetic interference shielding. Journal of Materials Chemistry A. 2015;3(9):4983-4991.
54. Gopakumar DA, Pai AR, Pottathara YB, Pasquini D, Morais LC, Khalil H.P.S A, Nzihou A, Thomas S. Flexible papers derived from polypyrrole deposited cellulose nanofibers for enhanced electromagnetic interference shielding in gigahertz frequencies. J Appl Polym Sci. 2020;138(16):50262.
55. Gopakumar DA, Pai AR, Pottathara YB, Pasquini D, Carlos de Morais L, Luke M, Kalarikkal N, Grohens Y, Thomas S. Cellulose Nanofiber-Based Polyaniline Flexible Papers as Sustainable Microwave Absorbers in the X-Band. ACS applied materials & interfaces. 2018;10(23):20032-20043.
56. Fugetsu B, Sano E, Sunada M, Sambongi Y, Shibuya T, Wang X, Hiraki T. Electrical conductivity and electromagnetic interference shielding efficiency of carbon nanotube/cellulose composite paper. Carbon. 2008;46(9):1256-1258.
57. Lee T-W, Lee S-E, Jeong YG. Highly Effective Electromagnetic Interference Shielding Materials based on Silver Nanowire/Cellulose Papers. ACS applied materials & interfaces. 2016;8(20):13123-13132.
58. Parit M, Du H, Zhang X, Prather C, Adams M, Jiang Z. Polypyrrole and cellulose nanofiber based composite films with improved physical and electrical properties for electromagnetic shielding applications. Carbohydrate polymers. 2020;240:116304.
59. Tang L, Han J, Jiang Z, Chen S, Wang H. Flexible conductive polypyrrole nanocomposite membranes based on bacterial cellulose with amphiphobicity. Carbohydr Polym. 2015;117:230-235.
60. Marins JA, Soares BG, Fraga M, Müller D, Barra GMO. Self-supported bacterial cellulose polyaniline conducting membrane as electromagnetic interference shielding material: effect of the oxidizing agent. Cellulose. 2014;21(3):1409-1418.